Detailing renal hemodynamics and oxygenation in rats by a combined near-infrared spectroscopy and invasive probe approach

Grosenick, D., Cantow, K., Arakelyan, K., Wabnitz, H., Flemming, B., Skalweit, A., Ladwig, M., Macdonald, R., Niendorf, T., Seeliger, E.

Biomedical Optics Express
2015 FEB 01 ; 6(2): 309-323
2015 JAN 06 (first published online)
doi: 10.1364/BOE.6.000309

Publisher: The Optical Society (OSA)

Detailing renal hemodynamics and oxygenation in rats by a combined near-infrared spectroscopy and invasive probe approach

Dirk Grosenick,[1] Kathleen Cantow,[2] Karen Arakelyan,[2,3] Heidrun Wabnitz,[1] Bert Flemming,[2] Angela Skalweit,[2] Mechthild Ladwig,[2] Rainer Macdonald,[1] Thoralf Niendorf,[3] and Erdmann Seeliger[2,*]

[1]*Physikalisch-Technische Bundesanstalt (PTB), Berlin, Germany*
[2]*Institut für Vegetative Physiologie, Charité – Universitätsmedizin Berlin, Berlin, Germany*
[3]*Berlin Ultrahigh Field Facility (B.U.F.F.), Max Delbrueck Center for Molecular Medicine, Berlin, Germany*
*erdmann.seeliger@charite.de

Abstract: We hypothesize that combining quantitative near-infrared spectroscopy (NIRS) with established invasive techniques will enable advanced insights into renal hemodynamics and oxygenation in small animal models. We developed a NIRS technique to monitor absolute values of oxygenated and deoxygenated hemoglobin and of oxygen saturation of hemoglobin within the renal cortex of rats. This NIRS technique was combined with invasive methods to simultaneously record renal tissue oxygen tension and perfusion. The results of test procedures including occlusions of the aorta or the renal vein, hyperoxia, hypoxia, and hypercapnia demonstrated that the combined approach, by providing different but complementary information, enables a more comprehensive characterization of renal hemodynamics and oxygenation.

OCIS codes: (170.6510) Spectroscopy, tissue diagnostics; (170.2655) Functional monitoring and imaging; (170.6935) Tissue characterization.

References and links

1. N. H. Lameire, A. Bagga, D. Cruz, M. J. De, Z. Endre, J. A. Kellum, K. D. Liu, R. L. Mehta, N. Pannu, B. W. Van, and R. Vanholder, "Acute kidney injury: an increasing global concern," Lancet. **382**, 170-179 (2013).
2. L. S. Chawla, P. W. Eggers, R. A. Star, and P. L. Kimmel, "Acute kidney injury and chronic kidney disease as interconnected syndromes," N. Engl. J. Med. **371**, 58-66 (2014).
3. K. C. Leung, M. Tonelli, and M. T. James, "Chronic kidney disease following acute kidney injury-risk and outcomes," Nat. Rev. Nephrol. **9**, 77-85 (2013).
4. R. G. Evans, C. Ince, J. A. Joles, D. W. Smith, C. N. May, P. M. O'connor, and B. S. Gardiner, "Haemodynamic influences on kidney oxygenation: clinical implications of integrative physiology," Clin. Exp. Pharmacol. Physiol. **40**, 106-122 (2013).
5. E. Seeliger, M. Sendeski, C. S. Rihal, and P. B. Persson, "Contrast-induced kidney injury: mechanisms, risk factors, and prevention," Eur. Heart J. **33**, 2007-2015 (2012).
6. P. Singh, S. E. Ricksten, G. Bragadottir, B. Redfors, and L. Nordquist, "Renal oxygenation and haemodynamics in acute kidney injury and chronic kidney disease," Clin. Exp. Pharmacol. Physiol. **40**, 138-147 (2013).
7. J. Prowle, S. M. Bagshaw, and R. Bellomo, "Renal blood flow, fractional excretion of sodium and acute kidney injury: time for a new paradigm?," Curr. Opin. Crit Care. **18**, 585-592 (2012).
8. J. L. Zhang, G. Morrell, H. Rusinek, E. E. Sigmund, H. Chandarana, L. O. Lerman, P. V. Prasad, D. Niles, N. Artz, S. Fain, P. H. Vivier, A. K. Cheung, and V. S. Lee, "New magnetic resonance imaging methods in nephrology," Kidney Int. **85**, 768-778 (2014).
9. T. Niendorf, A. Pohlmann, K. Arakelyan, B. Flemming, K. Cantow, J. Hentschel, D. Grosenick, M. Ladwig, H. Reimann, S. Klix, S. Waiczies, and E. Seeliger, "How bold is blood oxygenation-dependent (BOLD) magnetic resonance imaging of the kidney? Opportunities, challenges and future directions," Acta Physiol (Oxf). doi: 10.1111/apha.12393, (2014).

10. A. Pohlmann, K. Cantow, J. Hentschel, K. Arakelyan, M. Ladwig, B. Flemming, U. Hoff, P. B. Persson, E. Seeliger, and T. Niendorf, "Linking non-invasive parametric MRI with invasive physiological measurements (MR-PHYSIOL): towards a hybrid and integrated approach for investigation of acute kidney injury in rats," Acta Physiol (Oxf). **207**, 673-689 (2013).
11. A. Pohlmann, K. Arakelyan, J. Hentschel, K. Cantow, B. Flemming, M. Ladwig, S. Waiczies, E. Seeliger, and T. Niendorf, "Detailing the relation between renal T2* and renal tissue pO2 using an integrated approach of parametric magnetic resonance imaging and invasive physiological measurements," Invest Radiol. **49**, 547-560 (2014).
12. R. G. Evans, B. S. Gardiner, D. W. Smith, and P. M. O'connor, "Methods for studying the physiology of kidney oxygenation," Clin. Exp. Pharmacol. Physiol. **35**, 1405-1412 (2008).
13. V. Rajan, B. Varghese, T. G. van Leeuwen, and W. Steenbergen, "Review of methodological developments in laser Doppler flowmetry," Lasers Med Sci. **24**, 269-283 (2009).
14. B. Jackson and D. E. Oken, "Internephron heterogeneity of filtration fraction and disparity between protein- and hematocrit-derived values," Kidney Int. **21**, 309-315 (1982).
15. R. G. Evans, B. S. Gardiner, D. W. Smith, and P. M. O'connor, "Intrarenal oxygenation: unique challenges and the biophysical basis of homeostasis," Am. J. Physiol Renal Physiol. **295**, F1259-F1270 (2008).
16. A. Abdelkader, J. Ho, C. P. Ow, G. A. Eppel, N. W. Rajapakse, M. P. Schlaich, and R. G. Evans, "Renal oxygenation in acute renal ischemia-reperfusion injury," Am. J. Physiol Renal Physiol. **306**, F1026-F1038 (2014).
17. A. P. Gibson, J. C. Hebden, and S. R. Arridge, "Recent advantages in diffuse optical imaging," Phys. Med. Biol. **50**, R1-R43 (2005).
18. T. Durduran, R. Choe, W. B. Baker, and A. G. Yodh, "Diffuse optics for tissue monitoring and tomography," Reports Prog. Phys. **73**, 076701 (2010).
19. M. Ferrari and V. Quaresima, "A brief review on the history of human functional near-infrared spectroscopy (fNIRS) development and fields of application," Neuroimage. **63**, 921-935 (2012).
20. S. Lloyd-Fox, A. Blasi, and C. E. Elwell, "Illuminating the developing brain: the past, present and future of functional near infrared spectroscopy," Neurosci. Biobehav. Rev. **34**, 269-284 (2010).
21. A. Torricelli, D. Contini, A. Pifferi, M. Caffini, R. Re, L. Zucchelli, and L. Spinelli, "Time domain functional NIRS imaging for human brain mapping," Neuroimage. **85**, 28-50 (2014).
22. S. Ueda, D. Roblyer, A. Cerussi, A. Durkin, A. Leproux, Y. Santoro, S. Xu, T. D. O'Sullivan, D. Hsiang, R. Mehta, J. Butler, and B. J. Tromberg, "Baseline tumor oxygen saturation correlates with a pathologic complete response in breast cancer patients undergoing neoadjuvant chemotherapy," Cancer Res. **72**, 4318-4328 (2012).
23. D. Grosenick, H. Wabnitz, K. T. Moesta, J. Mucke, P. M. Schlag, and H. Rinneber, "Time-domain scanning optical mammography: II. Optical properties and tissue parameters of 87 carcinomas," Phys. Med Biol. **50**, 2451-2468 (2005).
24. S. Jiang, B. W. Pogue, C. M. Carpenter, S. P. Poplack, W. A. Wells, C. A. Kogel, J. A. Forero, L. S. Muffly, G. N. Schwartz, K. D. Paulsen, and P. A. Kaufman, "Evaluation of breast tumor response to neoadjuvant chemotherapy with tomographic diffuse optical spectroscopy: case studies of tumor region-of-interest changes," Radiology. **252**, 551-560 (2009).
25. M. Ferrari, M. Muthalib, and V. Quaresima, "The use of near-infrared spectroscopy in understanding skeletal muscle physiology: recent developments," Philos. Transact. A Math. Phys. Eng Sci. **369**, 4577-4590 (2011).
26. M. Weiss, G. Schulz, I. Teller, A. Dullenkopf, A. Kolarova, H. Sailer, C. M. Dillier, H. U. Bucher, A. C. Gerber, and O. Baenziger, "Tissue oxygenation monitoring during major pediatric surgery using transcutaneous liver near infrared spectroscopy," Paediatr. Anaesth. **14**, 989-995 (2004).
27. G. E. Owens, K. King, J. G. Gurney, and J. R. Charpie, "Low renal oximetry correlates with acute kidney injury after infant cardiac surgery," Pediatr. Cardiol. **32**, 183-188 (2011).
28. A. Petrova and R. Mehta, "Near-infrared spectroscopy in the detection of regional tissue oxygenation during hypoxic events in preterm infants undergoing critical care," Pediatr. Crit Care Med. **7**, 449-454 (2006).
29. L. A. Ortmann, E. E. Fontenot, P. M. Seib, B. K. Eble, R. Brown, and A. T. Bhutta, "Use of near-infrared spectroscopy for estimation of renal oxygenation in children with heart disease," Pediatr. Cardiol. **32**, 748-753 (2011).
30. C. G. Scully, N. Mitrou, B. Braam, W. A. Cupples, and K. H. Chon, "Detecting physiological systems with laser speckle perfusion imaging of the renal cortex," Am. J. Physiol Regul. Integr. Comp Physiol. **304**, R929-R939 (2013).
31. R. Bezemer, M. Legrand, E. Klijn, M. Heger, I. C. Post, T. M. van Gulik, D. Payen, and C. Ince, "Real-time assessment of renal cortical microvascular perfusion heterogeneities using near-infrared laser speckle imaging," Opt. Express. **18**, 15054-15061 (2010).
32. R. N. Raman, C. D. Pivetti, D. L. Matthews, C. Troppmann, and S. G. Demos, "A non-contact method and instrumentation to monitor renal ischemia and reperfusion with optical spectroscopy," Opt. Express. **17**, 894-905 (2009).
33. D. L. Vaughan, Y. A. Wickramasinghe, G. I. Russell, M. S. Thorniley, R. F. Houston, E. Ruban, and P. Rolfe, "Near infrared spectroscopy: blood and tissue oxygenation in renal ischemia-reperfusion in rats," Int. J. Angiol. **4**, 25-30 (1995).

34. W. Krause, P. Muschick, and U. Kruger, "Use of near-infrared reflection spectroscopy to study the effects of X-ray contrast media on renal tolerance in rats: effects of a prostacyclin analogue and of phosphodiesterase inhibitors," Invest Radiol. **37**, 698-705 (2002).
35. E. Seeliger, B. Flemming, T. Wronski, M. Ladwig, K. Arakelyan, M. Godes, M. Mockel, and P. B. Persson, "Viscosity of contrast media perturbs renal hemodynamics," J Am Soc Nephrol. **18**, 2912-2920 (2007).
36. E. Seeliger, K. Cantow, K. Arakelyan, M. Ladwig, P. B. Persson, and B. Flemming, "Low-dose nitrite alleviates early effects of an X-ray contrast medium on renal hemodynamics and oxygenation in rats," Invest Radiol. **49**, 70-77 (2014).
37. H. Wabnitz, M. Moeller, H. Liebert, H. Obrig, J. Steinbrink, and R. MacDonald, "Time-resolved near-infrared spectroscopy and imaging of the adult human brain," Adv. Exp Med Biol. **662**, 143-148 (2010).
38. D. Grosenick, O. Steinkellner, H. Wabnitz, R. MacDonald, T. Niendorf, K. Cantow, B. Flemming, and E. Seeliger, "Near-infrared spectroscopy of renal tissue in vivo," Proc. of SPIE **8578**, 85781P (2013).
39. J. R. Mourant, T. Fuselier, J. Boyer, M. Johnson, and I. J. Bigio, "Predictions and measurements of scattering and absorption over broad wavelength in tissue phantomes," Appl. Opt. **36**, 949-953 (1997).
40. W. R. Inch, J. A. McCredie, R. R. Knispel, R. T. Thompson, and M. M. Pintar, "Water content and proton spin relaxation time for neoplastic and non-neoplastic tissues from mice and humans," J. Natl. Cancer Inst. **52**, 353-356 (1974).
41. M. Mesradi, A. Genoux, V. Cuplov, H. D. Abi, S. Jan, I. Buvat, and F. Pain, "Experimental and analytical comparative study of optical coefficient of fresh and frozen rat tissues," J. Biomed Opt. **18**, 117010 (2013).
42. M. Solonenko, R. Cheung, T. M. Busch, A. Kachur, G. M. Griffin, T. Vulcan, T. C. Zhu, H. W. Wang, S. M. Hahn, and A. G. Yodh, "In vivo reflectance measurement of optical properties, blood oxygenation and motexafin lutetium uptake in canine large bowels, kidneys and prostates," Phys. Med Biol. **47**, 857-873 (2002).
43. T. Johannes, E. G. Mik, and C. Ince, "Dual-wavelength phosphorimetry for determination of cortical and subcortical microvascular oxygenation in rat kidney," J. Appl. Physiol. **100**, 1301-1310 (2006).
44. C. F. Cartheuser, "Standard and pH-affected hemoglobin-O2 binding curves of Sprague-Dawley rats under normal and shifted P50 conditions," Comp Biochem. Physiol Comp Physiol. **106**, 775-782 (1993).
45. D. J. Faber, M. C. Aalders, E. G. Mik, B. A. Hooper, M. J. van Gemert, and T. G. van Leeuwen, "Oxygen saturation-dependent absorption and scattering of blood," Phys. Rev. Lett. **93**, 028102 (2004).
46. B. Flemming, E. Seeliger, T. Wronski, K. Steer, N. Arenz, and P. B. Persson, "Oxygen and renal hemodynamics in the conscious rat," J. Am. Soc. Nephrol. **11**, 18-24 (2000).
47. P. Kumar, "Systemic effects resulting from carotid body stimulation," Adv. Exp. Med Biol. **648**, 223-233 (2009).
48. S. Lahiri and R. E. Forster, "CO2/H(+) sensing: peripheral and central chemoreception," Int. J. Biochem. Cell Biol. **35**, 1413-1435 (2003).
49. V. Vallon, B. Muhlbauer, and H. Osswald, "Adenosine and kidney function," Physiol Rev. **86**, 901-940 (2006).

1. Introduction

Acute kidney injury (AKI) is a frequent complication in hospitalized patients that can be triggered by a variety of causes including renal ischemic events, sepsis, shock of various origins, and administration of nephrotoxic substances. Although potentially reversible, AKI is one of the leading causes of in-hospital mortality, and patients who recover from AKI are predisposed to the development of chronic kidney disease (CKD) [1-3]. The pathophysiology of AKI is not completely understood, yet renal hypoxia resulting from imbalance between oxygen delivery and oxygen consumption is widely considered a pathophysiological key element of AKI and its progression to CKD [2,4-7]. This notion is largely based on experimental studies in animal models of kidney diseases that made use of quantitative invasive techniques for measurements of renal hemodynamics and oxygenation. Non-invasive methods applicable in patient studies, in particular, functional magnetic resonance imaging (MRI) including blood oxygenation level-dependent (BOLD) MRI can provide surrogate parameters for renal perfusion and blood oxygenation [8,9]. However, as calibration of these MRI parameters against the “gold standard” invasive techniques is still in its infancy, invasive studies in animal models remain essential for elucidating the role of hypoperfusion and hypoxia in renal disorders [9-11].

Well established invasive techniques comprise i) absolute measurement of total renal blood flow (RBF; in mL/min) by means of ultrasound transit time difference probes attached to the renal artery, ii) absolute measurements of regional tissue partial pressure of oxygen

(pO_2; in mmHg) by means of either Clark-type microelectrodes or fluorescence-quenching optodes, and iii) measurements of changes in regional tissue perfusion (erythrocyte flux) by means of laser-Doppler-probes [10,12]. Notwithstanding the utility and success of these techniques for characterization of renal hemodynamics and oxygenation, they have inherent methodological shortcomings. Laser-Doppler probes combine assessments of the average velocity of erythrocytes' movements and of the amount of erythrocytes per tissue volume to calculate a rough estimate of blood perfusion [10,13]. Yet even in the absence of changes in blood flow, the amount of erythrocytes per tissue volume may change considerably due to i) changes in systemic hematocrit e.g. during hemodilution, ii) changes in local hematocrit related to e.g. the phenomenon of plasma skimming, and changes in the vascular volume fraction that occur iii) via passive circular distension of vessels following changes in the transmural pressure gradient or iv) by active vasomotion [9,14]. The pO_2 probes, both the Clark electrodes and the quenching optodes, measure tissue oxygenation. The relationship between renal tissue oxygenation and renal blood oxygenation is quite variable because of the effects of arterio-venous shunt diffusion of oxygen and of plasma skimming [9,15]. Thus, even if blood oxygenation of systemic arterial blood (and renal venous blood) is measured from blood samples or by intravascular probes, the oxygenation of blood within the intrarenal vessels cannot be assessed [16].

Near-infrared spectroscopy (NIRS) is able to detect changes in the amount of oxygenated (oxy) and deoxygenated (deoxy) hemoglobin (Hb) per tissue volume. NIRS can even provide absolute values of these parameters as well as oxygen saturation of Hb (StO_2) [17,18]. NIRS has been applied in numerous investigations on humans including functional imaging of the adult or neonate brain [19-21], characterization of breast tissue and tumors *in vivo* [22-24], examination of muscle tissue [25], and non-invasive monitoring of hepatic oxygenation [26] and renal oxygenation in neonates and infants [27-29]

NIRS has also been applied in research on small animals. With regard to the kidney, there is a limited number of reports referring to the assessment of hemodynamics and oxygenation using optical methods. Laser-speckle imaging was used to examine intrarenal perfusion in rats [30,31]. The observation of NADH fluorescence after excitation with UV light is an approach to assess renal tissue hypoxia [32]. In an early NIRS application changes in oxyHb per tissue volume of the exposed kidney of rats were monitored during an ischemia/reperfusion intervention [33]. This study run the caveat that the tissues' strong light scattering was not taken into account so that qualitative estimates of the changes in oxygenation were provided only. In another NIRS study, a commercial reflection spectrometer was used to monitor relative changes of Hb per tissue volume and StO_2 in the renal cortex of rats upon administration of X-ray contrast agents [34].

Recognizing the need for detailing renal hemodynamics and oxygenation we hypothesize that combining quantitative NIRS with established invasive techniques provides different but complementary information. This synergy will enable a more comprehensive characterization of renal hemodynamics and oxygenation. Thus, we developed a NIRS device tailored for the investigation of the cortex of exposed rat kidneys *in vivo* and implemented a hybrid approach that allows simultaneous measurement of oxyHb, deoxyHb, tissue pO_2 and local perfusion in the renal cortex as well as total RBF and arterial blood pressure (ABP) in rats. To test our hypothesis, we used an array of dedicated test procedures including occlusion of the suprarenal aorta and the renal vein, changes in the inspiratory fraction of oxygen (FiO_2) and carbon dioxide ($FiCO_2$), and administration of adenosine.

2. Material and methods

Investigations were performed on a total of 13 male, 3-4 months old, Wistar rats (average body mass 350 g; Harlan-Winkelmann, Borchen, Germany). The studies were approved by Berlin's animal welfare administration in accordance with the German Animal Welfare Act.

2.1 Surgical preparation and invasive measurements

The rats were prepared as previously described in detail [35,36]. Briefly, the rats were anesthetized by urethane (20%, 6 ml/kg BM i.p.; Sigma-Aldrich, Steinheim, Germany) and breathed spontaneously via a tracheal cannula. A catheter was inserted into the left common carotid artery with its tip in the thoracic aorta to serve for continuous infusion of isotonic saline (1 ml/h) and for administration of adenosine. Another catheter was inserted into the femoral artery to monitor ABP and for continuous saline infusion (1 ml/h). A transit time flow probe (1RB, Transonic Systems, Ithaca, NY) was positioned around the left renal artery for measurement of RBF. A combined laser-Doppler-flux- and pO_2-quenching-probe (OxyFlo/OxyLite, Oxford Optronics, Oxford, UK) was inserted by means of a micromanipulator into the renal cortex with the tip being positioned about 1.5 mm below the renal capsule. The combined probe enables simultaneous monitoring of the flux of erythrocytes and of pO_2 within the tissue subjacent to the probe's tip. An inflatable cuff was positioned around the aorta above the renal arteries to permit aortic occlusions, and a smooth surgical twine armed with silastic tubing was positioned around the left renal vein to permit renal venous occlusions. During surgery and examination the abdominal cavity was filled with isotonic saline (37°C).

Data on ABP, RBF, cortical laser flux and tissue pO_2 were recorded at 50 Hz and later transformed into 1 Hz by means of a sliding average algorithm. To distinguish changes in flow and flux induced by ABP changes via passive vessel distension from those due to vasomotor actions, conductance values were calculated by dividing flow/flux data by ABP: renal vascular conductance (RVC) = RBF/ABP, cortical vascular conductance (CVC) = cortical laser flux/ABP.

2.2 Near-infrared spectroscopy setup

Multi-distance measurements of diffusely reflected light from the uncovered kidney were performed with a time-domain NIRS setup [37,38] which is schematically shown in Fig. 1. Three picosecond diode lasers were used as light sources with emission wavelength of 690 nm, 800 nm, and 830 nm. After passing filter wheels the laser beams were coupled into optical fibers of 50 µm core diameter which were combined in a common Sub Miniature A (SMA) ferrule. This connector was coupled to a 200 µm multimode fiber (numerical aperture NA = 0.22) guiding the light to the kidney. We used a fiber probe with one source fiber and four detector fibers (200 µm core diameter, NA 0.22) being linearly arranged. The source-detector separations were 2, 4, 6 and 8 mm. As illustrated in Fig. 1, the penetration depth increases according to the increasing source-detector separation.

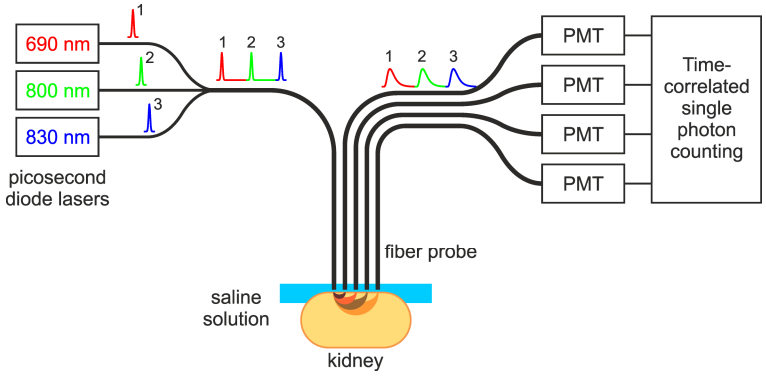

Fig. 1. Schematic view of the NIRS setup (PMT = photomultiplier tube).

The detection fibers were connected to cooled photomultipliers with GaAs photocathodes. The diffusely reflected light was recorded by time-correlated single photon counting. The

laser pulse trains at the three wavelengths were delayed against each other by about 7.5 ns. This multiplexing scheme was utilized to distinguish the wavelengths at each detector without spectral filtering and to easily subtract ambient background light. The time-resolution of our setup (400 ps to 600 ps for the different wavelengths) was not sufficient for a time-domain analysis of tissue optical properties at these short source-detector separations. We derived the time-integrated spatially-resolved reflectance for each wavelength by calculating the integrals of the corresponding photon time-of-flight distributions. Data acquisition was performed with a temporal resolution of 50 ms. In order to reduce the effects of respiration (~ 1.5 Hz) on the detected intensities a sliding average algorithm was used with an average time interval of 1 s.

The fiber probe was placed about 0.5 mm above the ventral surface of the uncovered left kidney by using a micromanipulator. The probe tip was continuously immersed in the saline filling the abdominal cavity.

2.3 Tests interventions

Invasive data and NIRS data were measured simultaneously. After recording of baseline data, the following test interventions were performed. 1) Aortic occlusion: by rapidly inflating the aortic cuff, the arterial blood inflow into the kidney was stopped; after 3 min of arterial occlusion, the cuff was rapidly opened which was followed by a recovery period of 10 min (n=13 rats). 2) Renal vein occlusion: by rapidly closing the surgical twine around the renal vein, the venous blood outflow from the kidney was stopped; after 3 min of venous occlusion, the twine was rapidly released which was followed by a recovery period of 10 min (n=10 rats, in the other three rats the vein could not successfully be occluded). 3) Hyperoxia: by increasing the FiO_2 from 21% (normoxia) to 100%, hyperoxia was induced and maintained for 6 min, followed by a recovery period of 10 min (n=13 rats). 4) Hypoxia: by decreasing the FiO_2 from 21% to 10%, hypoxia was induced and maintained for 2 min, followed by a recovery period of 10 min (n=8 rats, for the other 5 rats, hypoxia had to be terminated already within the first minute due to excessive hypotensive effects). 5) Hypercapnia: by increasing the $FiCO_2$ from about 0% (normocapnia) to 5%, hypercapnia was induced and maintained for 6 min, followed by a recovery period of 10 min (n=12 rats, for one rat delivery of CO_2 to the inspiratory gas was not successful). A Capnomac AGM-103 (Datex GE, Chalfont, UK) was used to monitor FiO_2 and $FiCO_2$ 6) Administration of adenosine: adenosine (15.4 µg/kg BM) was injected into the thoracic aorta, followed by 5 min recovery (n=12 rats, for the first animal this investigation was not carried out).

Thereafter, a NIRS reference measurement was performed for each animal by placing the fiber probe on the surface of a solid phantom with known optical properties.

2.4 Calculation of total hemoglobin and oxygen saturation of hemoglobin

The spatially-resolved NIRS reflectance data were analyzed employing a Monte Carlo model of light propagation in tissue. This model was used to describe the diffuse reflectance of light as a function of the absorption coefficient μ_a and the reduced scattering coefficient μ_s' of the medium. Since the depth penetration of light in our setup was mainly limited to the cortical tissue, the medium was assumed to be homogeneous. A reference measurement on a solid phantom was used to determine the sensitivity factors relating measured photon counts with photon flux densities given by the model for each detector at each of the three wavelengths λ. Generally, only four independent parameters are needed to calculate the spatially-resolved diffuse reflectance at the three wavelengths: the reduced scattering coefficient μ_s' at a selected wavelength λ_0 (in our case λ_0 = 800 nm), the scatter power coefficient b [39] which describes the decrease of the scattering coefficient with increasing wavelength, the total amount of hemoglobin per tissue volume tHb and the oxygen saturation of hemoglobin StO_2. The reduced scattering coefficients at the other two wavelengths entering the Monte Carlo model can then be calculated from $\mu_s'(\lambda_0)$ and b by the scatter power law [39]:

$$\mu_s'(\lambda) = \mu_s'(\lambda_0)(\lambda/\lambda_0)^{-b} \quad (1)$$

The related absorption coefficients can be derived from *tHb* and StO_2 using the equation:

$$\mu_a(\lambda) = tHb\left(\varepsilon_{\text{deoxyHb}}(\lambda)(1-StO_2) + \varepsilon_{\text{oxyHb}}(\lambda)\, StO_2\right) \ln 10 + V\mu_{a,H2O}(\lambda) \quad (2)$$

Here $\varepsilon_{\text{deoxyHb}}$ and $\varepsilon_{\text{oxyHb}}$ denote the molar decadic absorption coefficients of deoxyHb and oxyHb, respectively. The term $V\mu_{a,H2O}$ accounts for the absorption of water in the tissue where V is the water volume fraction, and $\mu_{a,H2O}$ is the absorption coefficient of pure water. Since the contribution of water to the renal tissue absorption is small compared to that of oxyHb and deoxyHb at the wavelengths used in our NIRS setup, we cannot reliably derive V from the measurements. To take the small contribution of water into account, we assume a constant water fraction of 75% as a representative value for the renal cortex [40]. As can be seen from Eq. (2), the oxygen saturation was calculated by assuming that oxyHb and deoxyHb are the only significant contributors to the total Hb; other Hb derivatives were neglected.

When deriving the four independent parameters for the baseline periods before and between the various interventions of each animal we found a large intra-individual spread of the scatter power coefficient *b*. Since the physiological conditions for a particular animal are about the same during all baseline periods due to the reversibility of the applied test interventions, this coefficient is expected to be almost constant during the baseline periods. When *b* is systematically varied in the physiologically expected range from 1 to 2 [41], we see that its estimation from our measurements is ill-conditioned because of the limited number of optical wavelengths. On the other side, the influence of *b* on the results for tHb and StO_2 is small: the corresponding StO_2 baseline values change by about 5 % only, and the values for tHb are barely affected. Therefore, we decided to use the baseline data of all animals to determine an average value of *b*, and to apply this value throughout the further analysis to determine tHb and StO_2 for each animal. Changes in the scattering properties of the tissue during the interventions are included in this approach by the scattering coefficients in Eq. (1).

In order to derive the average scatter power coefficient the baseline reflection data for each animal were averaged over a 10 s time window. These data were fitted by the Monte Carlo model to estimate preliminary reduced scattering and absorption coefficients for the various baseline periods for each wavelength. We calculated the medians of the preliminary reduced scattering coefficients for the 13 animals and used these data to determine the average scatter power coefficient b_{ave} from Eq. (1). This average value was fixed, and the preliminary reduced scattering coefficients were used to derive $\mu_s'(\lambda_0)$ in Eq. (1) for each animal. These values together with the global scatter power coefficient b_{ave} were taken to define the animal specific baseline values of μ_s' at the three wavelengths. The corresponding baseline absorption coefficients were then obtained by fitting the shape of the measured spatially-resolved reflection with the Monte Carlo model for each baseline data set and each wavelength separately.

The baseline optical properties obtained in this way were used to determine improved sensitivity factors for each stimulation period. Finally, the time courses for each intervention were analyzed using the three parameters μ_s'(800 nm), *tHb* and StO_2 as free fit parameters, whereby Eqs. (1) and (2) were taken to derive the other quantities. In this way the noise of the results could be considerably reduced.

2.5 Statistical analysis

Baseline values are given as mean values and standard deviations (SD). Furthermore, we calculated the median and the median absolute deviation (MAD) which are more robust against outliers. Results for the time courses measured during the interventions are depicted as relative changes (group mean ± standard error of mean (SEM)) obtained by relating the

absolute data during a given intervention to the absolute data obtained immediately before the respective intervention.

3. Results

3.1 Baseline values

Baseline data of total Hb per tissue volume (tHb), O_2 saturation of Hb (StO_2), reduced scattering (μ_s') and absorption coefficients (μ_a) derived from NIRS, and renal blood flow (RBF), blood pressure (ABP), renal vascular conductance (RVC), and tissue partial pressure of O_2 (pO_2) measured by invasive techniques are given in Tab. 1. Since laser-fluxmetry enables to assess changes only, no absolute data on cortical flux and conductance are given.

Table 1. Baseline values (n=13 rats) of parameters derived from NIRS and invasive measurements

Quantity	Unit	Mean	Standard deviation	Median	MAD
tHb	µmol/l	334	68	340	35
StO_2	%	63.7	5.1	62.4	2.4
μ_s'(690 nm)	cm^{-1}	12.2	1.6	11.5	0.8
μ_s'(800 nm)	cm^{-1}	10.2	1.4	9.5	0.7
μ_s'(830 nm)	cm^{-1}	9.7	1.3	9.1	0.7
μ_a(690 nm)	cm^{-1}	0.71	0.16	0.78	0.08
μ_a(800 nm)	cm^{-1}	0.64	0.12	0.65	0.04
μ_a(830 nm)	cm^{-1}	0.69	0.14	0.70	0.10
RBF	ml/min	3.10	0.89	3.28	0.37
ABP	mmHg	94.0	14.5	89.5	2.9
RVC	ml min^{-1} $mmHg^{-1}$	0.0334	0.0097	0.0350	0.0021
pO_2	mmHg	11.1	8.6	10.2	4.8

The average amount of tHb per tissue volume was 334 µmol/l (SD 68 µmol/l), the average StO_2 was 63.7% (SD 5.0%). Generally, deviations between median and mean values in Tab. 1 are small indicating that there are no substantial outliers. To compare the MAD values with the standard deviations one should use the 1.48-fold MAD value which corresponds to the standard deviation for a Gaussian distribution. The accordingly scaled MAD values are smaller by around 30% than the standard deviations, with a few exceptions. The average value b_{ave} of the scatter power coefficient amounted to 1.25. As will be discussed below, data obtained by NIRS refer to the cortex of the kidney.

3.2 Aortic and renal venous occlusion

Fig. 2 shows the relative changes of total RBF, tHb, laser flux, StO_2 and tissue pO_2 in the cortex for the aortic and the renal venous occlusion. ABP and vascular conductance are not depicted since ABP was measured via a femoral artery catheter (thus about zero during the aortic occlusion), and conductance cannot be determined during occlusions.

Upon the occlusion of the aortic cuff, inflow of arterial blood into the kidney immediately ceased: RBF that was measured by the flow probe attached to the renal artery, dropped abruptly and approached zero flow. Likewise, cortical flux decreased abruptly. At the same time, cortical tHb rapidly decreased by about 30%. After about 20 s, tHb started to increase gradually, whereas RBF and flux remained almost zero throughout the occlusion. The StO_2 of cortical blood decreased rapidly by about 38%, which was followed by a very slight further decrease throughout the occlusion. The cortical tissue pO_2 also decreased rapidly; it approached about zero and remained at this level. Upon the release of the aortic occlusion, RBF and cortical flux increased rapidly to about 60% of pre-occlusion levels, followed by slow increase until approaching baseline. Cortical tHb rapidly increased, reaching an overshoot of about 18% above baseline, then slowly decreased toward pre-occlusion level.

Cortical StO_2 recovery was somewhat faster than that of cortical flux. The recovery of tissue pO_2 was markedly slower than that of StO_2.

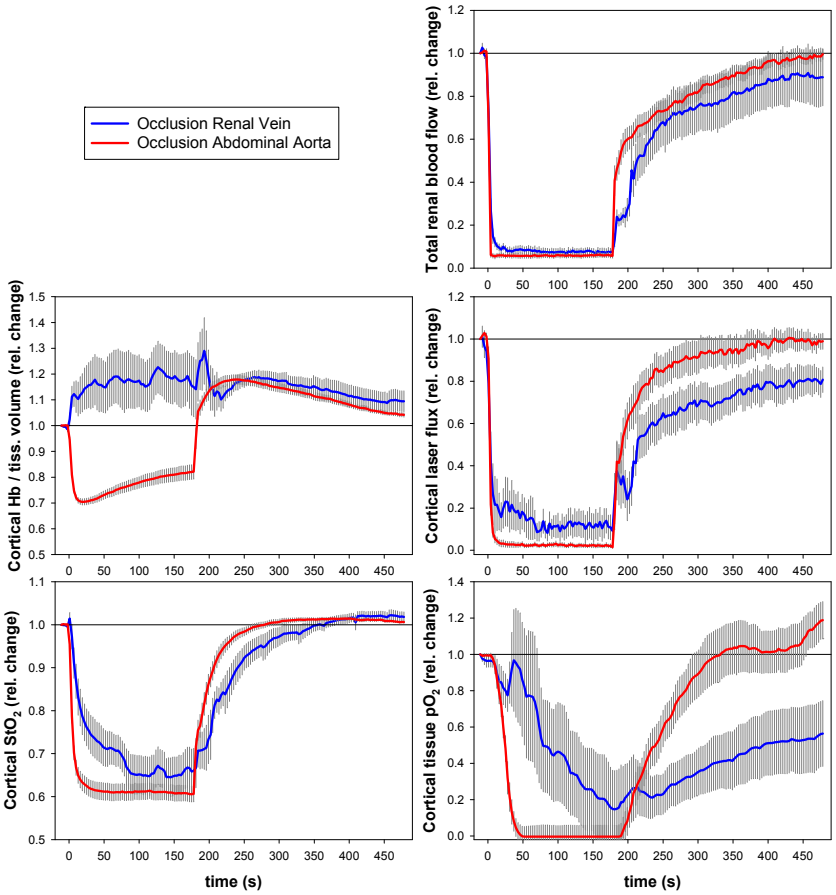

Fig. 2. Time courses of relative changes of total renal blood flow, total cortical Hb per tissue volume, cortical laser flux, cortical StO_2, and cortical tissue pO_2 during and following occlusion of either the abdominal aorta or the renal vein. Data are given as mean ± SEM.

With the occlusion of the renal vein, RBF that reflects arterial inflow of blood into the kidney approached zero somewhat slower as compared to the aortic occlusion. Cortical flux dropped even slower and did not reach the low level observed during aortic occlusion. Contrary to aortic occlusion, tHb rapidly increased rather than decreased upon the onset of venous occlusion. tHb continued to increase slightly during the occlusion reaching about 20% above baseline. StO_2 and, even more, pO_2 decreased much slower than upon the aortic occlusion. Upon the release of the venous occlusion, recovery of RBF, flux, and StO_2 were somewhat slower, and recovery of pO_2 was much slower than upon release of the aortic occlusion. Cortical tHb slowly returned to baseline.

3.3 Hyperoxic, hypoxic, and hypercapnic interventions

Hyperoxia (FiO_2=100%) caused an increase of ABP by up to 20%, hypoxia (FiO_2=10%) a decrease by up to 35%, whereas hypercapnia ($FiCO_2$=5%) barely changed ABP (Fig. 3). Hyperoxia led to a meager increase in RBF and a decrease in cortical vascular conductance by up to 10%, hypoxia to a decrease in RBF of up to 30% and an increase in CVC by up to 40%;

hypercapnia barely changed these parameters. Hyperoxia resulted in a small decrease in tHb, hypoxia in a small increase, hypercapnia did not change tHb.

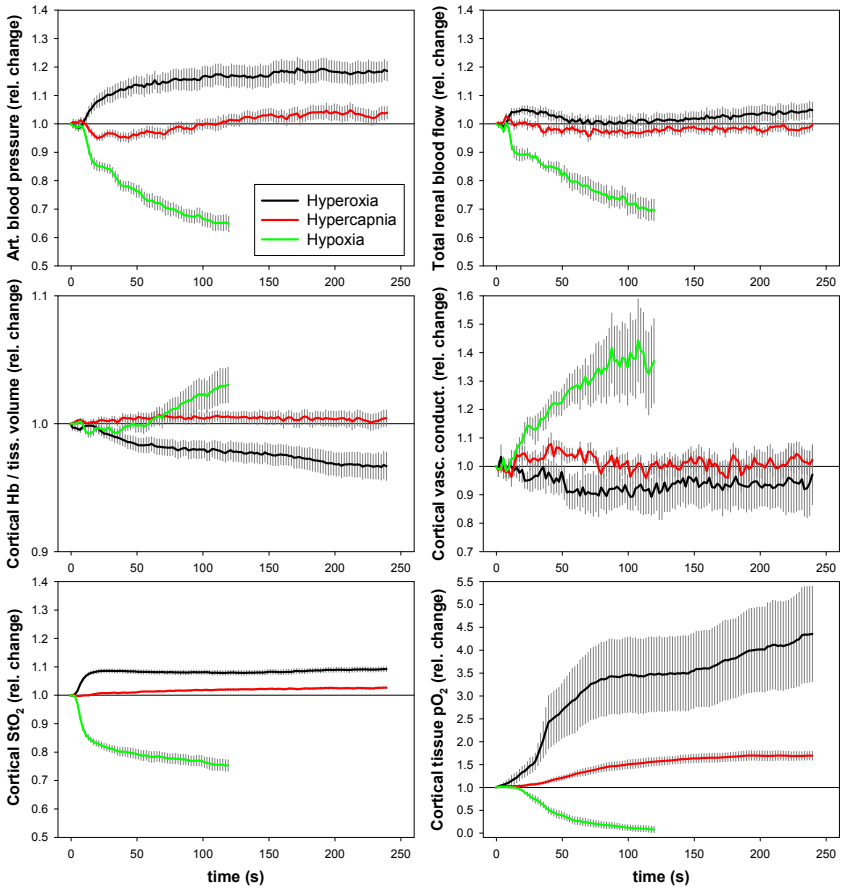

Fig. 3. Time courses of relative changes of arterial blood pressure, total renal blood flow, total cortical Hb per tissue volume, cortical vascular conductance, cortical StO_2, and cortical tissue pO_2 upon changes in the inspiratory gas mixture from room air to either hyperoxia (FiO_2=100%), hypoxia (FiO_2=10%), or hypercapnia ($FiCO_2$=5%). Data are given as mean ± SEM.

Hyperoxia resulted in a rapid increase in StO_2 by up to 8% and a slower increase in pO_2 that reached values more than four-fold as high as baseline. Hypoxia led to a decrease in StO_2 by up to 25% and a slower decrease in pO_2 by up to 90%. Hypercapnia resulted in a meager increase in StO_2 yet increased pO_2 by up to 65%.

3.4 Administration of adenosine

The bolus injection of adenosine into the thoracic aorta caused a transient but short overshoot followed by a rapid drop in ABP by about 25% and in RBF by about 38%. Both parameters approached baseline after about 30 s with RBF even exceeding baseline (Fig. 4). CVC dropped by about 18%; after about 10 s it increased again, followed by a small overshoot before approaching baseline. Cortical tHb dipped by about 6%, regained baseline within 20 s, and showed a slight overshoot versus baseline. The time course of StO_2 was similar to that of tHb. Unlike StO_2, pO_2 started to decrease much later (about 18 s after adenosine injection), reached a nadir of about 12% below baseline and regained baseline about 90 s after injection only.

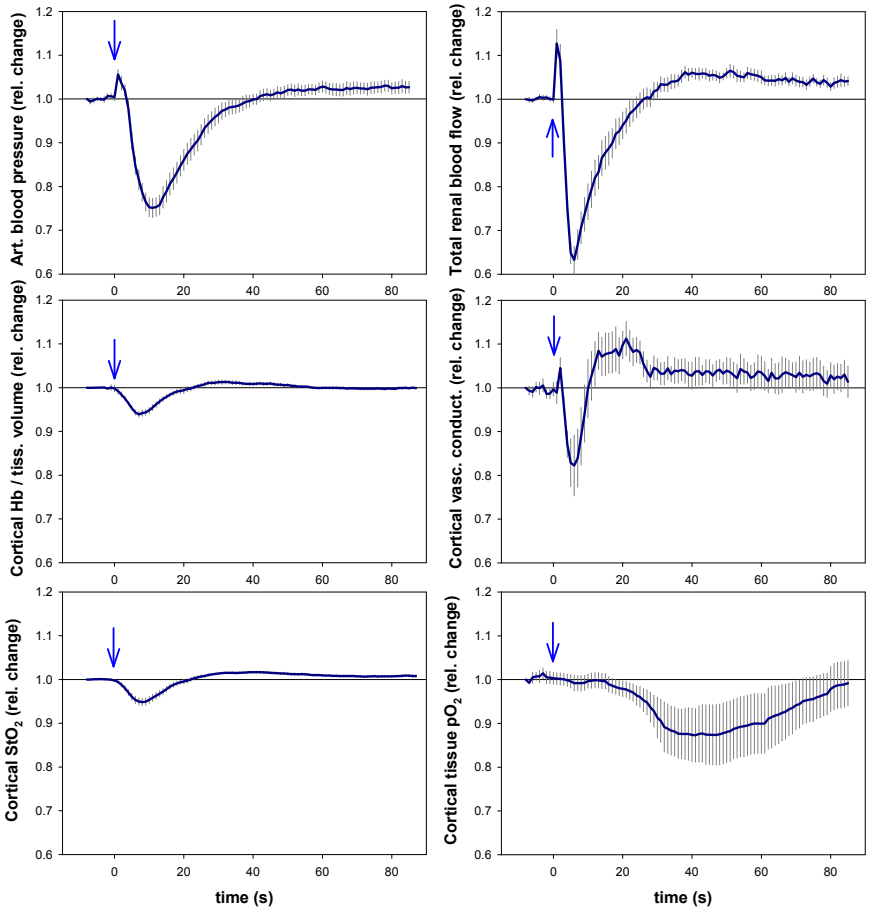

Fig. 4. Time courses of relative changes of arterial blood pressure, total renal blood flow, total cortical Hb per tissue volume, cortical vascular conductance, cortical StO_2, and cortical tissue pO_2 upon bolus injection (arrow) of adenosine into the thoracic aorta. Data are given as mean ± SEM.

4. Discussion and conclusions

The proposed NIRS technique enabled determination of absolute values of the total amount of Hb per renal cortical tissue volume and of the StO_2 in the cortical vessels of rats *in vivo* with high temporal resolution. The hybrid approach of NIRS with invasive methods affords simultaneous monitoring of tissue pO_2 and local perfusion in the renal cortex as well as total RBF and ABP. This approach proved capable to enable a more comprehensive characterization of renal hemodynamics and oxygenation.

With the NIRS technique, tHb, StO_2, and the related optical properties were quantified (see Tab. 1). The tHb values represent the amount of Hb molecules per tissue volume (in µmol/l). Results for StO_2 (in %) represent average values for the blood of all vessels lying within the investigated volume of the renal cortex, i.e., vessels that range from arteries through capillaries to veins. Our work adds to the literature by providing for the first time *in vivo* data on absolute tHb and absolute StO_2 of the rat kidney versus previous reports which were limited to relative changes of these parameters [33,34]. Our results on tHb (mean 334 µmol/l, SD 68 µmol/l) accord with results reported for the kidney of canines (mean 340 µmol/l, SD 92 µmol/l) [42]. StO_2 of intrarenal blood in canines was slightly higher (mean 70%, SD 21%) versus our data derived from rats (mean 63. 7%, SD 5.1%), whereby the

interindividual variation in the rat data is considerably smaller. Johannes et al. used a phosphorimetric method to measure blood pO_2 in the rat kidney; averaged over all vessel types, cortical blood pO_2 amounted to about 60 mmHg [43]. According to the oxyHb dissociation curve of rats, blood pO_2 of 60 mmHg corresponds with StO_2 of about 65% [44]. Assuming that no major shifts of the curve would take place in the renal cortex, our StO_2 values thus correspond well with the average cortical blood pO_2 reported by Johannes et al. [43]. Our assumption of a constant volume fraction of water (75%) has a minor effect on the results only. A change of the water volume fraction to 95% or down to 50% would affect tHb by about 3 µmol/l and StO_2 by about 0.3% only.

The reduced scattering coefficient of the canine renal tissue was given as mean 19.6 cm^{-1} (SD 4.0 cm^{-1}) at 730 nm [42], which is about 50% larger than our result for the rat at 690 nm (see Tab. 1). Data on scattering properties of rat kidneys are available from *in vitro* measurements only: Mesradi et al. obtained values of about 10 cm^{-1} at 690 nm (SD about 0.3 cm^{-1}) from 6 kidney slices of 3 rats [41], which is slightly smaller than our result. Our *in vivo* absorption coefficients are larger (0.71 cm^{-1} at 690 nm) than those reported from the *in vitro* study (about 0.5 cm^{-1} between 650 and 700 nm). This is plausible since the *in vitro* preparation entails partial loss of intrarenal blood. This reduced blood content should mainly affect the absorption coefficient. The impact on scattering properties should be small. Our scatter power coefficient (1.25) is somewhat smaller than the *in vitro* coefficient (1.63) [41]. However, if we used a scatter power coefficient of 1.63 instead of 1.25, this would result in a minor increase in StO_2 from 64% to just about 66%, and would barely affect our tHb value.

Red blood cells act as strong light scatterers [45]. Since the number of erythrocytes per tissue volume was altered by the interventions, we observed corresponding temporal changes in the scattering properties of the renal cortex (not shown here). In particular, the decrease in the amount of erythrocytes during the aortic occlusions and its increase during the venous occlusions were reflected in the observed temporal decrease (arterial occlusion) or increase (venous occlusion) of the reduced scattering coefficients at the three wavelengths. To a minor part, the observed alterations of the scattering properties could also be caused by changes of StO_2, since the scattering properties of red blood cells are known to depend on oxygen saturation [45]. On the other hand, the scatter power coefficient of whole blood in the NIR does not depend on oxygen saturation [45]. Hence, our assumption that the scatter power coefficient does not change during the interventions should not really influence the results for tHb and StO_2.

The banana-shaped areas in Fig. 1 illustrate the average volumes which are sampled optically by the four detector fiber setting. Since a homogeneous medium was assumed, the results on optical properties and Hb parameters represent average values over these four sub-volumes. The optical properties derived in this way can be used to estimate the penetration depth of the light. To this end, we used our Monte Carlo model to calculate the most probable photon trajectories between the position of the source and each of the detector fibers. For our largest source-detector distance (8 mm) the deepest point of the trajectory lies approximately 2 mm below the surface of the kidney so that our fiber probes support sampling of the cortical layer of the kidney.

The simultaneous measurements by NIRS and invasive probes yielded complementary information about renal hemodynamics and oxygenation as demonstrated by the test interventions. Suprarenal aortic and renal venous occlusions emulate clinical conditions in which deficient renal perfusion results in deterioration of intrarenal oxygenation. If maintained for longer periods of time these conditions can cause AKI. The rationale for performing both of these tests was that aortic occlusion and renal venous occlusion were anticipated to have similar effects with regard to renal perfusion and oxygenation, yet opposing effects with regard to intrarenal blood volume. With the onset of aortic occlusion the inflow of blood into the kidney is abruptly stopped while outflow via the renal vein continues until pressures in intrarenal vessels and in the vena cava are equalized [11]. With the onset of

renal venous occlusion, outflow of blood is abruptly stopped while inflow via the artery does not cease until the arterial pressure-induced distension of intrarenal vessels is counterbalanced by the resistance of the renal tissue including the rather tough capsula. Accordingly, RBF as monitored by the probe attached to the renal artery shows a somewhat slower approach to zero upon venous than upon aortic occlusion (see Fig. 2). The degrees of the opposing changes of intrarenal blood volume, however, become only clear from the NIRS-derived data on cortical tHb: at the onset of aortic occlusion, cortical tHb decreased by about 30%, at the onset of venous occlusion, tHb increased by about 12%. These NIRS data, furthermore, provide a lucid explanation for the observation that the laser-Doppler-signal is less reduced during the venous than the aortic occlusion. It is a known limitation of laser-fluxmetry that it relies on the amount of erythrocytes per tissue volume to calculate an estimate of perfusion [10,13].

As expected, the opposing changes of renal blood volume had an impact on renal oxygenation. Yet the effects proved surprisingly large. NIRS-derived StO_2 of cortical blood decreased rapidly upon aortic occlusion but decreased markedly slower and to a lesser extent during venous occlusion (see Fig. 2). Even more pronounced were the differences in cortical tissue pO_2. Renal O_2 consumption is probably the same during aortic and venous occlusions. Yet, the transiently maintained inflow of oxygenated blood at the onset of venous occlusion increases the intrarenal reservoir of O_2. In terms of absolute values of StO_2, with a baseline value of about 65% (cf. Table 1), StO_2 reached a bottom value of 39% during aortic occlusion and of 45% during venous occlusion. In both cases, aortic and venous occlusions, the decrease in tissue pO_2 was slower but much larger than that in StO_2 (see Fig. 2). Tissue pO_2 primarily reflects the balance between O_2 supply and O_2 consumption. The vast majority of O_2 is consumed by tubular epithelial cells for energy-dependent reabsorption processes. Because of the arterio-venous shunt diffusion of O_2, blood pO_2 and StO_2 in intrarenal arterial and venous vessels exceed those in the capillaries as well as tissue pO_2 under baseline conditions already [4,10,15]. In the early phase of the occlusions tubular reabsorption and, thus, O_2 consumption continues. The occlusions result in an immediate (aortic occlusion) or somewhat delayed (venous occlusion) arrest of blood in the renal vessels such that the ongoing O_2 demand can only be met by increasing the O_2 extraction from blood within the capillaries. This lowers blood pO_2 and StO_2 in the capillaries, yet does barely affect blood pO_2 and StO_2 in all the larger vessels [11]. Consequently, NIRS-derived StO_2 that represents the average StO_2 of all vessels within the investigated volume and the tissue pO_2 data measured by the optodes provide different but complementary information on renal oxygenation.

An additional intriguing result obtained by NIRS was that cortical tHb, after the steep drop at the onset of aortic occlusion, gradually increased again during the occlusion (see Fig. 2). The most probable explanation is that renal hypoxia induces dilation of intrarenal vessels [36,46], which results in a backflow of blood from the extrarenal veins into the kidney. A similar trend of increasing tHb throughout the venous occlusion may indicate that hypoxic vasodilation also enabled a small inflow of blood into the kidney, in this case via the renal artery. With the release of the aortic occlusion, massive arterial inflow into the dilated vessels results in an overshoot of tHb of up to 15%, i.e., to a similar extent as the one accumulated during the venous occlusion.

The hyperoxic, hypoxic, and hypercapnic test procedures were chosen because they primarily alter blood oxygenation. Hyperoxia led to an increase in StO_2 of about 8%, whereas tissue pO_2 increased to more than 400% of the baseline value (see Fig. 3). This result is expected since most of the Hb in arterial blood is already O_2 saturated under normoxic conditions. Setting FiO_2 to 100% can lift StO_2 in arterial blood only by a small degree. However, this maneuver induces a substantial increase in pO_2 of arterial blood. This enhances the driving force for diffusion of O_2 from vessels to tissue as well as from arteries to veins [4,10,15]. As a consequence, the increase in renal tissue pO_2 is substantial while that of NIRS-derived StO_2 – mostly attributable to increased venous StO_2 – is small [11]. While primarily altering blood oxygenation, the hyperoxic stimulus has also secondary effects: it results in

vasoconstriction in renal as well as extrarenal vascular beds [46]. This manifests itself in the ABP increase, the slight CVC decrease and the tHb decrease.

Hypoxia is a condition with particular relevance for the pathophysiology of AKI. The primary effect of reducing the FiO_2 to 10% is a decrease in oxygenation of arterial blood with the consequent reduction in renal O_2 supply. With ongoing O_2 consumption, this does *per se* result in a decrease in renal tissue pO_2. Yet renal O_2 supply is further diminished by hypoxia-induced vasodilation [36,46] with ensuing decrease in ABP (see Fig. 3). Despite the dilation of renal vessels indicated by both the increase in CVC and the increase in tHb, RBF also decreased by up to 30%. The dual effects on O_2 supply led to an increasing mismatch with O_2 consumption, ultimately reducing tissue pO_2 by up to 90%. Cortical StO_2 as monitored by NIRS declined by up to 25% only. The major reason behind this difference is again related to the arterio-venous O_2 shunt: increased O_2 extraction in the capillaries reduce blood pO_2 in the venous vessels thereby increasing the driving force for arterio-venous diffusion, which in turn further lowers capillary and tissue oxygenation [15]. An additional effect probably contributes to the different extent of tissue pO_2 versus StO_2 decrease. Arterial hypoxemia, via arterial chemorectors, triggers an increase in ventilation that reduces the blood's CO_2 content [47]. The ensuing leftward shift of the oxyHb dissociation curve hinders the release of O_2 which *per se* results in lower blood and tissue pO_2 and higher StO_2.

With the hypercapnic stimulus (increasing $FiCO_2$ to 5%) we aimed at the opposite effect, namely a rightward shift of the oxyHb dissociation curve. This would *per se* result in a decrease in StO_2 and an increase in blood and tissue pO_2. In fact, tissue pO_2 increased by up to 65% while StO_2 barely changed (see Fig. 3). The major reason that StO_2 did not decrease is that increased CO_2 content of arterial blood is a very strong stimulus for ventilation, again mediated by arterial chemoreceptors [47,48]. It can be concluded that the 65% increase in tissue pO_2 results from both the enhanced release of O_2 due to the rightward shift of the oxyHb dissociation curve and the increased ventilation.

The rationale behind the adenosine bolus injection was that this metabolite induces vasoconstriction in the renal cortex but vasodilation in the majority of extrarenal vascular beds [49]. The extrarenal vasodilation is mirrored by the decrease in ABP (see Fig. 4). In conjunction with the shorter lasting renal vasoconstriction mirrored in CVC and tHb, this reduced RBF by up to 38% for about 30 s. Intriguingly, StO_2 dipped shortly along with CVC and tHb, whereas tissue pO_2 started to decrease only 10 s after the nadir in StO_2 and remained reduced for a longer time. As RBF and StO_2 are above rather than below baseline values at this time, the pO_2 response could just reflect a delay between reduced O_2 supply and reduced tissue oxygenation. However, in addition to its vasomotor effects, adenosine stimulates proximal tubular reabsorption [49]. It is conceivable that the late pO_2 decrease may, in part, reflect an increase in O_2 consumption. Here again the combination of NIRS and invasively measured parameters provided complementary information.

Notwithstanding the success and capabilities of the NIRS technique employed, there is room for further improvements. The present results on tHb and StO_2 rely on the assumption that the sampled cortical volume is homogeneous. However, the underlying raw data of spatially-resolved reflectance for the four detection fibers refer to the different banana-like sub-volumes and, in particular, to different depths within the tissue. The development of a layered model for data analysis should enable to distinguish temporal changes in the outer and inner cortex. With the present reflection geometry, the investigations are limited to the renal cortex of the rats. An increase of the penetration depth could be realized by positioning source and detection fibers on different sides of the kidney. With such a setup, data could be recorded in transmission or by a combined reflection/transmission approach.

Our approach with combined NIRS and established invasive techniques to study renal hemodynamics and oxygenation could further be complemented by other techniques such as phosphorimetric techniques to measure intrarenal blood pO_2 [43], laser speckle imaging to

measure intrarenal perfusion [31], NADH autofluorescence to assess cellular hypoxia [32], or invasive methods to monitor renal O_2 consumption [16].

Our NIRS technique could also serve to help calibrate BOLD-MRI. This non-invasive technique can probe blood oxygenation with high spatial and temporal resolution and whole kidney coverage. The surrogate parameter for blood oxygenation, the effective transversal relaxation time T_2* is related to the amount of deoxyHb per tissue volume [8,9]. To become a quantitative tool for probing renal hypoperfusion and hypoxia in renal disorders though, BOLD-MRI must be calibrated by means of other quantitative techniques. To approach this goal, pioneering studies in rats combined BOLD-MRI with invasive methods including pO_2-optodes and flow probes in a dedicated hybrid setup (MR-PHYSIOL) [10,11]. These studies revealed that the relationship between T_2* and tissue pO_2 is confounded by a number of factors including, but not limited to, the vascular volume fraction, the local hematocrit, shifts of the oxyHb dissociation curve, and the kidney's tubular volume fraction [9]. Since NIRS enables quantitative monitoring of the amount of Hb per tissue volume and of StO_2 it is an ideal candidate to unravel and quantify the contributions of several confounders.

To conclude, with the proposed NIRS technique absolute values of tHb per tissue volume and StO_2 can be obtained from the renal cortex of rats *in vivo* with high temporal resolution. This provides different but complementary data to those obtained by established invasive methods or BOLD-MRI. Combined approaches will be instrumental to elucidate the role of hemodynamics and oxygenation in AKI and its progression to CKD.

Acknowledgement

We would like to acknowledge Richard Schäfer, Ariane Anger and Andrea Gerhardt for expert technical assistance during measurements and data analysis. This work was supported in part by the German Research Foundation (Deutsche Forschungsgemeinschaft, research unit FOR 1368, grant numbers: NI 532/9-1, SE 998/3-1).